NANO LETTERS

2007
Vol. 7, No. 8
2183−2187

ZnO Nanotube Based Dye-Sensitized Solar Cells

Alex B. F. Martinson,[†,‡] Jeffrey W. Elam,[‡] Joseph T. Hupp,*[,†] and Michael J. Pellin[‡]

Northwestern University, 2145 Sheridan Road, Evanston, Illinois 60208, and Argonne National Laboratory, 9700 South Cass Avenue, Argonne, Illinois 60439

Received January 20, 2007; Revised Manuscript Received May 25, 2007

ABSTRACT

We introduce high surface area ZnO nanotube photoanodes templated by anodic aluminum oxide for use in dye-sensitized solar cells (DSSCs). Atomic layer deposition is utilized to coat pores conformally, providing a direct path for charge collection over tens of micrometers thickness. Compared to similar ZnO-based devices, ZnO nanotube cells show exceptional photovoltage and fill factors, in addition to power efficiencies up to 1.6%. The novel fabrication technique provides a facile, metal-oxide general route to well-defined DSSC photoanodes.

The good light-harvesting efficiency of the best dye-sensitized solar cells (DSSCs) is the product of a dye with moderate extinction and a photoanode of high surface area (∼1200 times the area of a flat electrode). This combination allows for ample absorbance over the majority of the visible spectrum with room for improvement in the red wavelengths.[1] In the most efficient cells, the photons intercepted by these molecular dyes create excitons that split on the tens of femtoseconds time scale resulting in charge separation efficiencies approaching unity.[2,3] The efficiency of the final step, charge collection, is governed by the difference between the rate of charge transport and the rate of charge recombination. In order to compete with relatively slow (millisecond) transport through the nanoparticle network, an exceedingly slow redox shuttle such as iodide/triiodide must be employed to hinder recombination.[4] Thus, prototypical DSSCs, based on TiO_2 and iodide/triiodide, exhibit very good electron collection, despite small apparent electron diffusion coefficients. This remarkable behavior is important in accounting for the record high efficiency (∼11%) of these cells.[1]

In order to push device performance beyond its current limits, a faster redox shuttle (that requires a smaller overpotential to reduce the oxidized dye) may be employed to increase the photovoltage (provided that dark current in not enhanced). Alternatively, a higher surface area framework would increase light-harvesting efficiency and, therefore, photocurrent. Successful implementation of either scenario will require slowing charge recombination. Methods to decrease the rate of parasitic reactions with the redox shuttle include inorganic barrier layers on the metal oxide framework and modification of the dyes.[5−7] A faster redox shuttle or higher surface area framework may also require faster charge transport though the metal oxide framework to allow for complete charge collection under cell operating conditions. Indeed, simply replacing iodide/triiodide with faster shuttles, but without implementing other changes, has been shown to *decrease* power conversion efficiencies due to the emergence of electron collection problems.[8,9] To this end, several novel photoanode architectures have been fabricated, including but not limited to hydrothermally grown ZnO nanorod arrays, electrodeposited ZnO platelets, and TiO_2 pores formed via titanium anodization.[10−12] Due to their lower trap density and more direct path to the current collecting electrode, arrays of nominally one-dimensional (1-D) nanostructures are expected to speed charge migration without adversely affecting recombination. In the most successful application of this idea to date, a 1.5% efficient ZnO nanorod array has been shown to exhibit much faster transport than nanoparticle networks.[10,13,14] The efficiency of the nanorod devices, however, is limited by low light-harvesting efficiency. Increasing the surface area of the nanorod array depends on growing higher aspect ratio rods via hydrothermal methods, which remains a significant technological challenge.[15]

Here we introduce a new photoanode design featuring very high aspect ratio substructures and having the potential for roughness factors (RFs) greater than 1000 (although our initial studies are limited to RF ≤ 450). The design implementation strategy combines anodic aluminum oxide (AAO) templating and atomic layer deposition (ALD) to yield oriented arrays of electrically interconnected semiconductor nanotubes. Because it is both a stepwise and conformal coating technique, ALD provides exceptional control

* Corresponding author: e-mail, J-hupp@northwestern.edu; telephone, 1-(847)-491-3504; fax, 1-(847)-467-1425.
[†] Northwestern University.
[‡] Argonne National Laboratory.

10.1021/nl070160+ CCC: $37.00 © 2007 American Chemical Society
Published on Web 06/29/2007

over nanoscale device composition and architecture. The large number of metal oxides accessible by ALD[16] (including, but not limited to, TiO_2, ZnO, SnO_2, ZrO_2, and NiO) makes the technique potentially very widely applicable for the development of new photoelectrodes. In this Letter we demonstrate the viability of ZnO versions of these structures as dye-sensitized electrodes by characterizing their morphology, light-harvesting efficiency, and photovoltaic performance.

A nominally 60 μm thick membrane with 200 nm pores that is 25−50% porous (Anodisc, Whatman) was coated with ZnO by atomic layer deposition via alternate exposure to diethyl zinc and water at a temperature of 200 °C using reactant exposure times of 6 s and nitrogen purge periods of 5 s between exposures.[17] The membranes were fired at 400 °C in air for 30 min to increase crystallinity. A 1 μm thick electrode composed of transparent, conductive aluminum-doped zinc oxide (AZO) was deposited on one side by ALD. The commercial AAO membranes chosen for this study have pores that narrow to 20 nm within the last micrometer of thickness of one side. During AZO deposition, a steel fixture masked all but the small-pore face of the membrane. To improve the electrical contact to the AZO coating, 100 nm of Au was evaporated onto the coating along the edges of the AAO membrane.

After heating to 200 °C and subsequent cooling to 80 °C, the warm membranes were introduced to 0.5 mM $(Bu_4N)_2$-[Ru(4,4′-(COOH)-2,2′-bipyridine)$_2$(NCS)$_2$] ("N719", Dyesol, B2 dye) in ethanol for 30 min followed by a quick rinse with acetonitrile. A 50 μm thick Surlyn frame was sandwiched between the open-pore side of the membrane and a platinized fluorine-doped tin oxide (FTO) electrode. Light pressure was applied at 130 °C to seal the cell. A solution of 0.5 M LiI, 0.05 mM I_2, and 0.5 M *tert*-butylpyridine in 3-methoxypropionitrile was introduced into the cell via vacuum backfilling through a hole in the FTO electrode. Additional Surlyn and a microscope cover slip sealed the electrolyte into the cell. Monochromatic illumination was achieved through the excitation monochromator of a Jobin-Yvon fluorescence spectrometer. Incident photon-to-current efficiencies (IPCE) were measured with a CH Instruments 1202 potentiostat. Active areas were limited to 0.28 cm^2 by the Surlyn frame and were additionally masked from illumination by black electrical tape to the same size. AM1.5 efficiencies were measured on a class A solar cell analyzer from Spectra-Nova Technologies with a power of 906 W/m^2. To better understand charge collection, cells were also illuminated through the Pt/FTO electrode, which attenuated ∼20% of the light at visible wavelengths due mostly to Pt absorption. For an identical batch of photoanodes, dye loading was quantified on a Varian Cary 5000 by measuring the absorbance of N719 desorbed from the membranes by 10 mM KOH.

As an inert, robust, and colorless framework, anodic aluminum oxide is an ideal foundation for solar cell electrodes. A large amount of literature exists describing the theory and methodology for fabricating freestanding AAO membranes with hexagonally ordered pores ranging in size from 10 to 300 nm and pore densities in excess of 100 billion pores/cm^2.[18−20] For this study, commercial membranes were selected for their ready availability. Limitations of commercial membranes include ill-defined pore ordering, strong scattering of visible light, and restriction to only a few pore sizes and lengths. Geometric consideration of hexagonally arranged pores allows roughness factors to be estimated from

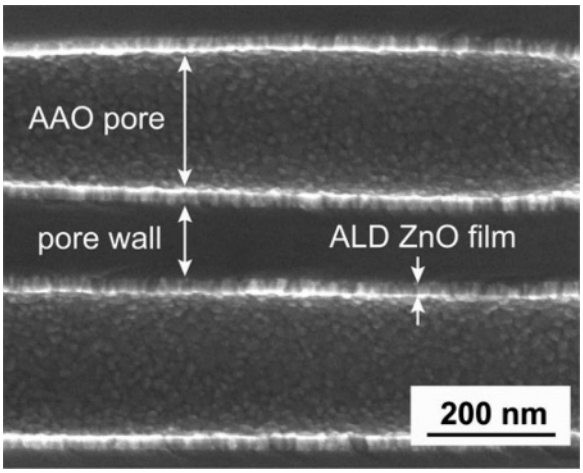

Figure 1. Cross-sectional SEM image of commercial AAO membrane pores coated with 20 nm of ZnO by ALD.

$$\mathrm{RF} = \frac{4\pi}{\sqrt{3}}\frac{rl}{d^2} \tag{1}$$

where r, l, and d are the pore radius, membrane thickness, and center-to-center pore spacing, respectively. Although poorly ordered, an average pore diameter of 210 nm, spacing of 329 nm, and length of 64 μm were estimated by scanning electron microscopy (SEM), giving RF ≈ 450. This compares well to the measured BET surface area of 487 cm^2/cm^2 of the membrane.

As expected for an ALD sequence entailing sufficient exposure times, the resulting polycrystalline ZnO film is continuous and conformal, Figure 1. Measurements of the resistance through the 64 μm thickness of the membrane (∼48 Ω, 8 nm thick ZnO) provide additional evidence that coatings span the length of the pores. As-deposited, ALD ZnO has numerous oxygen vacancies that make films moderately conductive and account for the relatively low resistance. The polycrystalline nature of the ZnO films may be directly observed by SEM and is corroborated by X-ray diffraction data. Both methods suggest a grain size of ∼20 nm.

As shown in Figure 2, a thick coating of AZO was applied selectively to one side of the membrane by ALD. The combination of narrow pore termini and short exposure times (0.15 s) prevented the typically conformal deposition technique from significantly coating the pore interiors.

As shown in Figure 3, reducing r by coating the pores reduces the dye loading, in agreement with surface area calculations. The peak absorbance is 0.71 at 500 nm for a 2 nm coating of ZnO and decreases with increasing thickness.

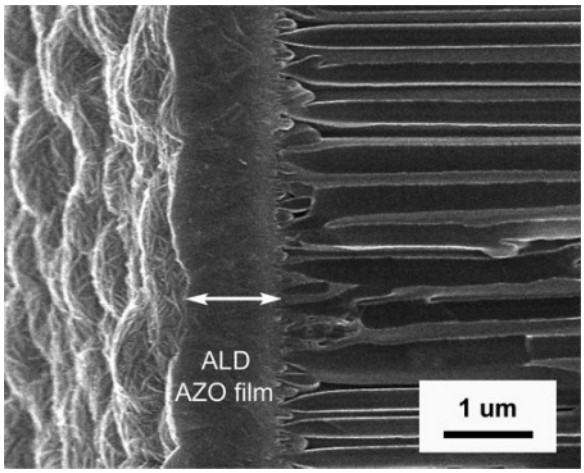

Figure 2. Cross-sectional SEM image of commercial AAO face coated with transparent conductive oxide AZO.

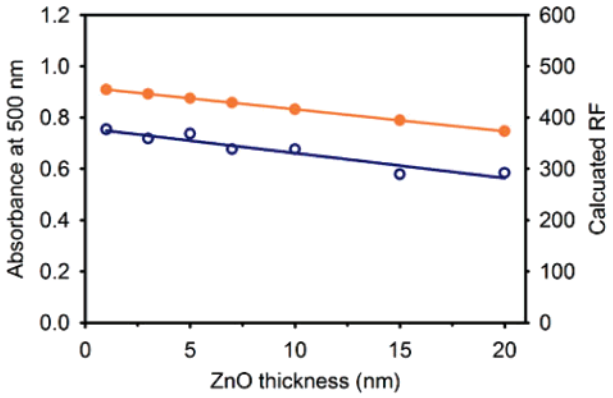

Figure 3. Absorbance of desorbed dye at 500 nm (blue, open symbols) and calculated roughness factor (orange, closed symbols). Lines are best linear fits to the data.

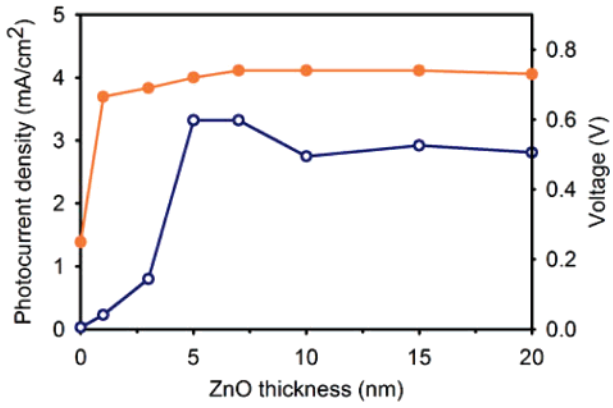

Figure 4. Short-circuit photocurrent (blue, open symbols) and open-circuit photovoltage (orange, closed symbols) as a function of ZnO wall thickness.

As expected, the modest RFs ($\sim^1/_3$ those of the best DSSCs) result in relatively low overall light-harvesting efficiencies that we expect to limit photocurrent densities.

Figure 4 shows the short-circuit photocurrent densities (J_{sc}) for a series of devices with increasing nanotube wall thickness. In the control device, lacking ZnO, J_{sc} is extremely low. This is not surprising given that the useful surface area is similar to that of a flat electrode. With the thinnest tube walls, relatively small amounts of charge are collected by the AZO electrode, most likely due to a combination of slow charge transport through the ZnO and accelerated recombination owing to high steady-state concentrations of dye-injected electrons. As the nanotube walls thicken, electrons flow more freely and J_{sc} rises sharply. Subsequent tapering with thicker walls is consistent with decreasing dye loading (Figure 3).

The photovoltage at open circuit (V_{oc}) rises sharply after deposition of only 1 nm of ZnO. The exceptionally low voltage in the absence of ZnO is likely caused by the direct contact of the redox shuttle with the heavily doped AZO layer, whose conduction band (in contrast to ZnO's) is unable to fix the cell photovoltage. The photovoltage increases with increasing ZnO wall thickness until it plateaus after 7 nm. This V_{oc} (739 mV) exceeds that of the highest previously reported ZnO DSSC photovoltages (ca. 670−710 mV).[10,21] The excellent photovoltage is most likely not a result of improved charge transport but a consequence of the low area of transparent conducting oxide (TCO) exposed in the new device geometry. While many TiO_2-based DSSCs employ a dense blocking layer or $TiCl_4$ treatment to inhibit the parasitic reaction of the redox shuttle at the TCO, there is little precedence for this type of passivation in ZnO systems. For the photoanodes of interest here, an increasing ZnO film thickness serves a second function, namely to narrow the nominally 20 nm pores directly adjacent to the TCO. An increase in photovoltage coincides with tapering these small pores until the photovoltage peaks around the thickness expected to completely restrict electrolyte access to the TCO. Inhibited recombination via the TCO in addition to a significantly smaller ($\sim^1/_3$) ZnO surface area for recombination, relative to nanoparticle films, may explain the superior V_{oc}. The V_{oc} value observed here, while high, is still about 200−260 mV less than the maximum theoretically obtainable based on the difference of redox-shuttle and dye-excited-state potentials. In principle, it should be possible to capture some fraction of the remaining 200−260 mV by suppressing dark current (slowing charge recombination). Deposition of a barrier layer[6] may be one way to achieve such a result.

Insight into the improvement of cell performance with increasing ZnO layer thickness may be obtained by investigating charge carrier lifetimes (electron/triiodide recombination times). Analysis of the photovoltage decay affords electron lifetimes (τ_n) related to the slope of the photovoltage vs time plot by the expression

$$\tau_n = \frac{k_B T}{q}\left(\frac{dV_{OC}}{dt}\right)^{-1} \quad (2)$$

where k_B is the Boltzmann constant, T is the absolute temperature, and q is the positive elementary charge.[22] Electron lifetimes as a function of photovoltage are shown for two ZnO film thicknesses, Figure 5. Compared to other ZnO devices, the photovoltage decays of the best ZnO nanotube devices are similar.[23] At equal potentials (0.6 V), electron lifetimes increase as a function of ZnO pore wall

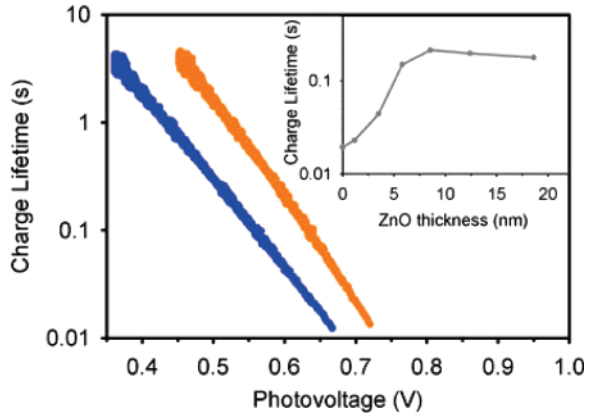

Figure 5. Charge lifetime vs photovoltage for a device with 4 nm pore wall (blue) and 9 nm pore wall (orange). Inset shows charge lifetimes as a function of pore wall thickness at equal cell potential (600 mV).

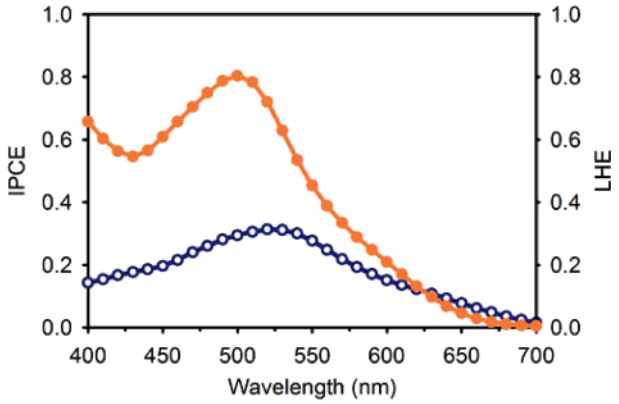

Figure 6. The incident photon-to-current efficiency (blue, open symbol) and light-harvesting efficiency (orange, closed symbols) of ZnO cell with 5 nm pore wall.

thickness up to 9 nm, inset Figure 5. The trend is striking and parallels the behavior shown in Figure 4 (i.e., increasing J_{sc} with increasing ZnO layer thickness). Whether this reflects an intrinsic change in ZnO reactivity with increasing thickness, or simply better blockage of electron recombination from exposed TCO, has yet to be established.

Figure 6 shows the peak in LHE at 500 nm, characteristic of N719. As expected for an electrode of modest surface area, a small fraction of the AM1.5 spectrum is absorbed by the cell. The peak incident photon-to-current efficiency (IPCE) occurs 20 nm red-shifted from the apparent LHE peak evaluated with desorbed dye. Necessarily neglected in the LHE evaluation are additional effects due to reflection and scattering by the commercial membranes.

Under AM1.5 illumination the most efficient cell gives a J_{sc} of 3.3 mA/cm^2, V_{oc} of 739 mV, and fill factor (FF) of 0.64, yielding an overall conversion efficiency of 1.6%, Figure 7. To our knowledge, the FF is the highest yet measured for a ZnO DSSC. Clearly, the overall efficiency of this system is limited primarily by the photocurrent. The relatively low photocurrent is a result of several factors including small RF, photoanode reflectivity/scattering, and either (or both) low injection yield + charge collection efficiency. In the most efficient DSSCs a scattering layer of

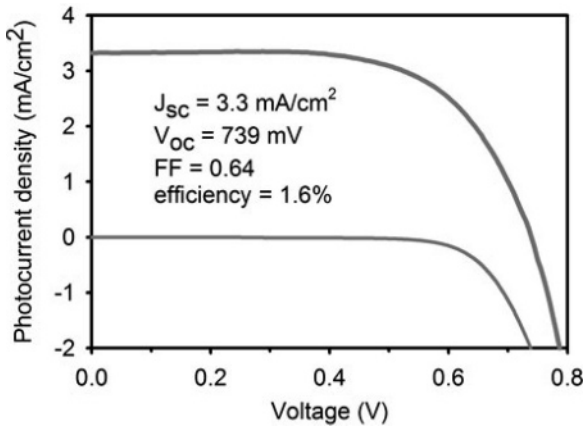

Figure 7. $I-V$ curve for the most efficient cell, 7 nm ZnO, under simulated AM1.5 illumination.

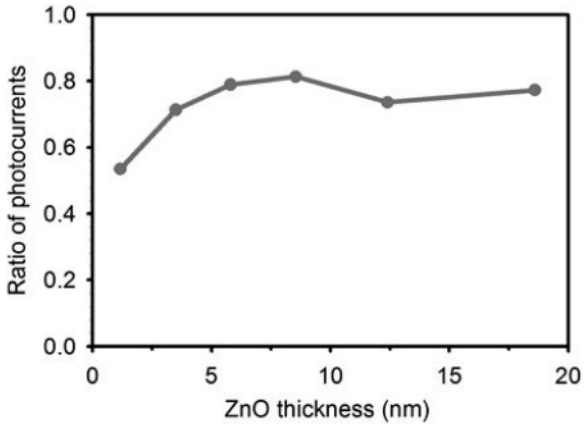

Figure 8. Ratio of photocurrents, backside vs frontside illumination. The ratio has *not* been corrected for light loss (ca. 20%) through the platinized counter electrode under backside illumination.

large particles is intentionally deposited on top of a transparent semiconductor network to reflect light back into the transparent electrode.[1] Yet photoanodes that are scattering throughout, as is the case in the current devices, show high reflectivity and poor light harvesting.[24] Finally, ZnO DSSCs generally exhibit much smaller absorbed photon-to-current efficiencies than do similar TiO_2 cells (implying inefficient electron injection and/or collection). We reasoned that the reduced dimensionality of the nanotube array electrodes, relative to nanoparticulate electrodes, would allow for efficient charge collection over long distances (50 μm) due to more rapid electron transport (as previously shown for nanorod arrays).[13,14] That the nanotube arrays indeed can collect charge with equal efficiency over the entire length of the tubes was established by evaluating photocurrent densities based on backside illumination, Figure 8. If correction for light losses of ca. 20% due to the dark electrode were to be made, identical J_{sc} values to front-side illumination would be obtained. As expected, the increase in collection efficiency correlates closely with the increase in electron lifetime.

In conclusion, ZnO nanotube arrays embedded in a porous alumina template by atomic layer deposition have been combined with AZO coatings to generate relatively high area photoelectrodes (RF = 350−450). The electrodes have been

incorporated into dye-sensitized solar cells where they display reasonable light-harvesting efficiency, excellent photovoltage, and good fill factors in addition to moderate power efficiency. While the new nanotube cells compare favorably with other ZnO-based DSSCs, increased surface area (ca. 3-fold or more) will clearly be needed in order to obtain overall energy conversion efficiencies approaching that of the best ZnO cells (4%).[21] Current work is focused on determining the extent to which the substantial optical + structural advantages of custom-made membranes can be translated into better photoelectrode performance. Finally, in contrast to other nominally 1-D photoanode assembly schemes, the ALD template approach should provide straightforward access to other high area semiconductor electrodes[5,25] including some previously inaccessible via traditional nanoparticle networks. Work on such systems is in progress.

Acknowledgment. The work at Northwestern is supported by the U.S. Department of Energy, Basic Energy Sciences Program, under Grant DE-FG02-87ER13808. Work at Argonne is supported by the U.S. Department of Energy, BES-Materials Sciences under Contract W-31-109-ENG-38. Electron microscopy was performed at the Electron Microscopy Center for Materials Research at Argonne National Laboratory, a U.S. Department of Energy Office of Science Laboratory operated under Contract No. DE-AC02-06CH11357 by UChicago Argonne, LLC. We thank Tobin Marks for use of the solar cell analyzer and Karen Mulfort for BET analysis.

References

(1) Gratzel, M. *Inorg. Chem.* **2005**, *44* (20), 6841−6851.
(2) Benko, G.; Yartsev, A. P.; Sundstrom, V. *Trends Opt. Photonics* **2002**, *72* (Thirteenth International Conference on Ultrafast Phenomena, 2002), 434−435.
(3) Kallioinen, J.; Benkoe, G.; Myllyperkioe, P.; Khriachtchev, L.; Skrman, B.; Wallenberg, R.; Tuomikoski, M.; Korppi-Tommola, J.; Sundstroem, V.; Yartsev, A. P. *J. Phys. Chem. B* **2004**, *108* (20), 6365−6373.
(4) Frank, A. J.; Kopidakis, N.; van de Lagemaat, J. *Coord. Chem. Rev.* **2004**, *248* (13−14), 1165−1179.
(5) Law, M.; Greene, L. E.; Radenovic, A.; Kuykendall, T.; Liphardt, J.; Yang, P. *J. Phys. Chem. B* **2006**, *110* (45), 22652−22663.
(6) Fabregat-Santiago, F.; Garcia-Canadas, J.; Palomares, E.; Clifford, J. N.; Haque, S. A.; Durrant, J. R.; Garcia-Belmonte, G.; Bisquert, J. *J. Appl. Phys.* **2004**, *96* (11), 6903−6907.
(7) Kroeze, J. E.; Hirata, N.; Koops, S.; Nazeeruddin, M. K.; Schmidt-Mende, L.; Gratzel, M.; Durrant, J. R. *J. Am. Chem. Soc.* **2006**, *128* (50), 16376−16383.
(8) Kruger, J.; Plass, R.; Gratzel, M.; Cameron, P. J.; Peter, L. M. *J. Phys. Chem. B* **2003**, *107* (31), 7536−7539.
(9) Gratzel, M. *MRS Bull.* **2005**, *30* (1), 23−27.
(10) Law, M.; Greene, L. E.; Johnson, J. C.; Saykally, R.; Yang, P. D. *Nat. Mater.* **2005**, *4* (6), 455−459.
(11) Yoshida, T.; Pauporté, T.; Lincot, D.; Oekermann, T.; Minoura, H. *J. Electrochem. Soc.* **2003**, *150*, (C608).
(12) Paulose, M.; Shankar, K.; Varghese, O. K.; Mor, G. K.; Grimes, C. A. *J. Phys. D*: *Appl. Phys.* **2006**, *39* (12), 2498−2503.
(13) Galoppini, E.; Rochford, J.; Chen, H.; Saraf, G.; Lu, Y.; Hagfeldt, A.; Boschloo, G. *J. Phys. Chem. B* **2006**, *110* (33), 16159−16161.
(14) Martinson, A. B. F.; McGarrah, J. E.; Parpia, M. O. K.; Hupp, J. T. *Phys. Chem. Chem. Phys.* **2006**, *8*, 4655 - 4659.
(15) Greene, L. E.; Yuhas, B. D.; Law, M.; Zitoun, D.; Yang, P. *Inorg. Chem.* **2006**, *45* (19), 7535−7543.
(16) Ritala, M.; Leskela, M. Atomic Layer Deposition. In *Handbook of Thin Film Materials*; Nalwa, H. S., Ed.; Academic Press: San Diego, CA, 2001; Vol. 1, p 103.
(17) Elam, J. W.; Routkevitch, D.; Mardilovich, P. P.; George, S. M. *Chem. Mater.* **2003**, *15* (18), 3507−3517.
(18) Li, A. P.; Müller, F.; Birner, A.; Nielsch, K.; Gösele, U. *J. Appl. Phys.* **1998**, *84*, 6023−6026.
(19) Masuda, H.; Yada, K.; Osaka, A. *Jpn. J. Appl. Phys.* **1998**, *37*, L1340−L1342.
(20) Lee, W.; Ji, R.; Gösele, U.; Nielsch, K. *Nat. Mater.* **2006**, *5*, 741−747.
(21) Kakiuchi, K.; Hosono, E.; Fujihara, S. *J. Photochem. Photobiol., A* **2006**, *179*, 81−86.
(22) Zaban, A.; Greenshtein, M.; Bisquert, J. *Chem. Phys. Chem.* **2003**, *4*, 859−864.
(23) Quintana, M.; Edvinsson, T.; Hagfeldt, A.; Boschloo, G. *J. Phys. Chem. C* **2007**, *111*, 1035−1041.
(24) Wang, Z.-S.; Kawauchi, H.; Kashima, T.; Arakawa, H. *Coord. Chem. Rev.* **2004**, *248* (13−14), 1381−1389.
(25) Elam, J. W.; Martinson, A. B. F.; Pellin, M. J.; Hupp, J. T. *Chem. Mater.* **2006**, *18* (15), 3571−3578.

NL070160+